Research Square

Preprints are preliminary reports that have not undergone peer review.
They should not be considered conclusive, used to inform clinical practice,
or referenced by the media as validated information.

Distinct Scaling Relationships of White-Light Facular and Ca II K Plage Areas with Sunspot Area over Solar Cycles 14--20

Jouni Takalo

jojuta@gmail.com

Research Article

Keywords:

Posted Date: November 13th, 2026

DOI: https://doi.org/10.21203/rs.3.rs-11535772/v1

License: This work is licensed under a Creative Commons Attribution 4.0 International License.
Read Full License

Additional Declarations: No competing interests reported.

Solar Physics
DOI: 10.1007/●●●●●-●●●-●●●-●●●●-●

Distinct Scaling Relationships of White-Light Facular and Ca II K Plage Areas with Sunspot Area over Solar Cycles 14–20

Jouni J. Takalo

© **The author(s) ●●●●**

Abstract We investigate how historical white-light facular and Ca II K plage areas scale with sunspot area over Solar Cycles 14–20. Monthly observations were constructed from the Greenwich Photo-Heliographic Results, the Kodaikanal Solar Observatory Ca II K plage-area series, and a cross-calibrated sunspot-area record, yielding 847 matched monthly values. We compared linear, saturating, and power-law relationships and evaluated their predictive performance using leave-one-solar-cycle-out cross-validation. The fitted power-law exponents are 0.382 for white-light faculae and 0.710 for Ca II K plages, indicating substantially stronger sublinear scaling in the facular record.
For facular area, the saturating model reduces the cross-validated root-mean-square error by 24.4% relative to the linear model. For plage area, the corresponding reduction is only 0.15%, while the power-law model provides a modest improvement of approximately 1.5%. The difference between the two diagnostics persists when the exceptionally active Solar Cycle 19 is excluded. Solar-cycle block bootstrap resampling further supports the observed contrast, although uncertainty estimates are limited by the seven available cycles.
These results show that historical white-light facular and Ca II K plage areas have distinct empirical relationships with sunspot area, with nonlinear saturation providing a substantially greater predictive advantage for the photospheric facular record.

Keywords: Sun: filaments; Sun: activity; Sun: magnetic field; Sun: sunspots; Sun: evolution

1. Introduction

Solar magnetic activity manifests itself through a variety of photospheric and chromospheric structures, including sunspots, faculae, and plages. Although these

Taivalkuja 12 b, FI-90910 Kontio
(e-mail: jojuta@gmail.com)

features are associated with magnetic fields emerging through the solar surface, they differ in their observational appearance, atmospheric formation heights, and sensitivity to magnetic flux. Sunspots are relatively dark photospheric structures associated with strong magnetic fields, whereas faculae and plages are generally observed as enhanced brightness in photospheric white-light observations and chromospheric Ca II K images, respectively. Their temporal evolution provides complementary information on the distribution and development of solar magnetic activity (Solanki et al. 2006; Yeo et al. 2020).

The relationship between dark sunspots and bright magnetic features is also important for understanding variations in solar irradiance. Sunspots produce a temporary reduction in solar brightness, while facular and network contributions can compensate for this effect and contribute to longer-term irradiance variations. Historical observations of sunspot and facular areas therefore provide valuable constraints on reconstructions of solar activity and radiative variability over timescales extending well beyond the availability of modern space-based measurements (Foukal and Lean 1990; Yeo et al. 2020; Chatzistergos et al. 2023).

Long-term photographic observations offer an opportunity to investigate these relationships across several solar cycles. The Royal Greenwich Observatory and its associated observing network produced extensive records of sunspot and white-light facular areas. These observations have been widely used in studies of historical solar activity, although the interpretation of the Greenwich facular record requires particular care because of the observational characteristics and potential inhomogeneities of the series (Foukal 1993). Chromospheric activity can be investigated using historical Ca II K spectroheliograms, among which the Kodaikanal Solar Observatory archive provides one of the longest observational records, extending from 1904 to 2007. The digitization and calibration of such archives have enabled quantitative investigations of plage areas and their long-term evolution (Priyal et al. 2014; Chatzistergos et al. 2020; Jha et al. 2024).

Previous studies have established that sunspot, facular, and plage areas are closely related, but their relationships need not be strictly linear. Early investigations already indicated differences between the behavior of photospheric faculae and chromospheric plages in relation to sunspot activity (Foukal 1996). Using Kodaikanal Ca II K observations and Greenwich sunspot data, Mandal et al. (2017) investigated the association between plages and sunspots. More recently, Chatzistergos et al. (2022a) examined the relationship between plage areas and sunspot areas and numbers using multiple historical Ca II K archives, highlighting the importance of nonlinear scaling and observational differences among datasets. Using modern observations, Yeo et al. (2020) also demonstrated that the relationship of facular and network contributions to sunspot activity is relevant to the interpretation of solar and stellar brightness variations.

Building on previous studies of sunspot–plage relationships, the present work directly compares the functional forms describing historical white-light facular and Ca II K plage areas against a common sunspot-area record, with particular emphasis on predictive performance across solar cycles. The two diagnostics sample different atmospheric layers and are obtained using different observational techniques. Consequently, their area–area relationships may exhibit different degrees of nonlinearity, even when both are associated with the same underlying

solar magnetic activity. It is therefore important to distinguish differences in scaling behavior from differences in absolute area calibration and measurement units.

In this study, we investigate the scaling of Greenwich white-light facular areas and Kodaikanal Ca II K plage areas with the cross-calibrated sunspot areas compiled by Mandal et al. (2020) over Solar Cycles 14–20. We construct a common monthly dataset and examine three empirical relationships: a linear model, a saturating model, and a power-law model. Rather than relying solely on goodness of fit within the full observational record, we evaluate the predictive performance of these models using leave-one-solar-cycle-out cross-validation. We further assess the sensitivity of the inferred relationships to individual solar cycles and to potentially problematic observational periods.

Our primary objective is to determine whether photospheric facular and chromospheric plage areas exhibit systematically different scaling behavior with sunspot area, and whether these differences remain stable across solar cycles. We also examine the influence of the exceptionally strong solar cycle 19, while keeping the principal focus on the comparative behavior of the two magnetic-activity diagnostics.

2. Data and Methods

2.1. Observational data

We investigate the relationships between three historical indicators of solar magnetic activity: photospheric white-light facular area, chromospheric Ca II K plage area, and sunspot area. The analysis covers solar cycles 14–20, corresponding approximately to the period 1904–1976. The study period is limited by the availability of the Greenwich white-light facular-area series used here, which ends in 1976, whereas the sunspot-area and Ca II K plage-area records extend beyond this date.

2.1.1. Sunspot and white-light facular area records

The photospheric sunspot and white-light facular areas were obtained from two related historical data products. The corrected sunspot area was taken from the daily cross-calibrated sunspot-area series compiled by Mandal et al. (2020), whereas the white-light facular area was extracted from the historical Greenwich Photoheliographic Results records. The original Greenwich Photo-heliographic Results document the historical procedures used to measure sunspot and white-light facular areas, including the contributions of different observatories and changes in measurement practices over time (Royal Observatory, Greenwich 1907, 1952; Royal Greenwich Observatory 1958).

Throughout this work, the corrected sunspot area is denoted by S, while the white-light facular area is denoted by F. Both quantities are expressed in millionths of the visible solar hemisphere (μHem).

The corrected sunspot areas account for the geometrical foreshortening of sunspots on the solar disk. The historical facular area series is treated as a

distinct observational quantity, and its definition and potential inhomogeneities are considered when interpreting the results (Foukal 1993).

2.1.2. Kodaikanal Ca II K plage areas

Chromospheric plage areas were obtained from the Kodaikanal Solar Observatory (KoSO) Ca II K photographic archive. We use the processed plage-area series associated with the reconstruction described by Jha et al. (2024), which covers the period 1904–2007.

The KoSO archive consists of digitized historical Ca II K spectroheliograms. The processing includes photometric calibration, compensation for large-scale image effects, and the identification of plage regions using image-contrast information.

The plage area is denoted by P and expressed in millionths of the solar disk (μDF). This differs from the area convention used for the sunspot and white-light facular areas (μHem). The original area units are retained throughout the analysis.

Consequently, the absolute numerical values of F and P are not directly compared. Instead, we compare the functional dependence of each quantity on sunspot area and the predictive performance of alternative empirical models.

2.2. Monthly data construction

To compare the three observational series on a common temporal basis, we constructed monthly records from the available daily and monthly data.

The daily corrected sunspot areas from Mandal et al. (2020) were first matched by observation date with the daily white-light facular areas from the Greenwich Photoheliographic Results. Monthly mean sunspot and facular areas were then calculated from the matched daily observations. Consequently, the monthly sunspot and facular values were based on the same set of available observation dates within each month.

For an area quantity X, the monthly mean was defined as

$$\overline{X}_m = \frac{1}{n_m} \sum_{d \in D_m} X_d, \tag{1}$$

where D_m denotes the set of matched observation dates in calendar month m, and n_m is the number of observations entering the monthly mean.

The KoSO Ca II K plage-area series was processed separately into monthly means. These monthly plage areas were subsequently matched with the monthly sunspot and facular areas by calendar year and month. Thus, the three monthly quantities refer to the same calendar month, but the KoSO observations were not necessarily obtained on the same individual days as the sunspot and facular observations.

Only months with at least 10 KoSO observation days were considered for inclusion. The final analysis further required finite values of all three area quantities, with non-negative sunspot and plage areas and strictly positive facular area, and was restricted to Solar Cycles 14–20.

The resulting dataset contains $N = 847$ monthly records. Each record includes the calendar year, month, solar-cycle assignment, corrected sunspot area, white-light facular area, and Ca II K plage area. We denote these monthly quantities by S_m, F_m, and P_m, respectively.

2.3. Empirical scaling models

We investigate whether the dependence of facular and plage areas on sunspot area can be described by the same functional form. Each model is fitted separately to the two response variables,

$$Y_m \in \{F_m, P_m\}, \tag{2}$$

using S_m as the explanatory variable.

Three empirical models are considered.

2.3.1. Linear model

The linear relationship is written as

$$Y(S) = a + bS, \tag{3}$$

where a is the intercept and b is the slope.

This model represents a constant incremental change in facular or plage area per unit increase in sunspot area.

2.3.2. Saturating model

To allow for a progressively weaker response at high sunspot areas, we use the saturating relationship

$$Y(S) = a + \frac{AS}{K + S}, \tag{4}$$

where a is the intercept, A controls the amplitude of the saturating component, and K is its characteristic sunspot-area scale.

For $K > 0$, the model approaches $a + A$ as S becomes large. Thus, it can represent a response that increases approximately linearly at low activity but gradually flattens at higher activity levels.

2.3.3. Power-law model

We also consider the power-law relationship

$$Y(S) = a + bS^{\alpha}, \tag{5}$$

where α is the scaling exponent.

An exponent $\alpha = 1$ corresponds to linear dependence apart from the intercept, whereas $0 < \alpha < 1$ represents sublinear scaling. The exponent provides a compact measure of the curvature of the area–area relationship and permits a comparison between the two observational diagnostics.

All three models are empirical descriptions of the observed relationships. Their intercepts are not assumed to represent a physically meaningful background area at zero sunspot activity. In particular, extrapolation beyond the observed sunspot-area range is avoided.

2.4. Model fitting and prediction errors

The models were fitted to the monthly observations by minimizing the sum of squared residuals. The linear model was fitted by ordinary least squares, whereas the saturating and power-law models were fitted by nonlinear least-squares minimization using multiple initial parameter estimates to reduce sensitivity to local minima.

Positivity constraints on the amplitude and scale parameters of the saturating model were enforced through parameter transformations. For the power-law model, the amplitude was constrained to be positive and the exponent was restricted to $0.10 < \alpha < 2.50$. The intercepts were left unconstrained.

For a set of N observations, the root-mean-square error (RMSE) is defined as

$$\mathrm{RMSE} = \sqrt{\frac{1}{N}\sum_{m=1}^{N}\left[Y_m - \widehat{Y}(S_m)\right]^2}, \tag{6}$$

where $\widehat{Y}(S_m)$ is the model prediction for observation m.

The RMSE is expressed in the units of the corresponding response variable: μHem for facular area and μDF for plage area. Therefore, absolute RMSE values are compared only between models fitted to the same response variable.

2.5. Leave-one-solar-cycle-out validation

An important objective is to assess whether a scaling relationship inferred from some solar cycles can predict observations from another cycle.

For this purpose, we employ leave-one-solar-cycle-out (LOCO) cross-validation. In each validation iteration, all monthly observations belonging to one solar cycle are excluded from the model fitting. The model is then fitted using the remaining cycles and applied to predict the observations of the excluded cycle. This procedure is repeated for each of solar cycles 14–20, so that every cycle serves once as an independent validation block.

The predictions from all held-out cycles are combined, and the overall cross-validated RMSE is calculated as

$$\mathrm{RMSE}_{\mathrm{LOCO}} = \sqrt{\frac{\sum_{c=14}^{20} \sum_{m \in M_c} \left[Y_m - \widehat{Y}_{-c}(S_m) \right]^2}{\sum_{c=14}^{20} |\mathcal{I}_c|}}, \tag{7}$$

where M_c denotes the set of monthly observations assigned to cycle c, and $\widehat{Y}_{-c}$ is the model fitted without that cycle. Unlike an ordinary in-sample goodness-of-fit comparison, LOCO validation evaluates the transferability of the empirical relationship between solar cycles.

To express the predictive benefit of a nonlinear model relative to the linear model, we define

$$G_{\mathrm{model}} = 100 \left(1 - \frac{\mathrm{RMSE}_{\mathrm{LOCO,model}}}{\mathrm{RMSE}_{\mathrm{LOCO,linear}}} \right) \%. \tag{8}$$

A positive value indicates an improvement over the linear model, whereas a negative value indicates poorer predictive performance.

2.6. Solar-cycle sensitivity and uncertainty

Because the observational record covers only seven solar cycles, monthly observations cannot be regarded as fully independent realizations of long-term solar activity. We therefore assess the robustness of the inferred scaling relationships using two complementary approaches.

First, we perform leave-one-cycle-out refitting of the power-law model. In this analysis, one solar cycle is excluded and the power-law parameters are re-estimated from the remaining cycles. The difference between the plage and facular scaling exponents is then calculated as

$$\Delta\alpha = \alpha_P - \alpha_F. \tag{9}$$

This sensitivity analysis is distinct from predictive LOCO validation: its purpose is to assess the dependence of the fitted exponents on individual cycles, rather than to estimate out-of-sample prediction error.

Second, we use a solar-cycle block bootstrap in which entire solar cycles, rather than individual months, are resampled with replacement. The same resampled cycle composition is used for both facular and plage areas, and cycles selected multiple times receive corresponding multiplicity weights. For each bootstrap realization, the power-law scaling exponents and the relative LOCO-RMSE improvements are recalculated using weighted least-squares fits. The nonlinear shape parameters are optimized by one-dimensional bounded minimization, while the remaining coefficients are obtained by weighted linear least squares. The bootstrap fits used the same bounds on the power-law exponent as the primary analysis and enforced non-negative amplitudes for both nonlinear models. The

saturating-model scale parameter was constrained to be positive. In the LOCO calculations, the held-out cycle is excluded from model fitting. We use 300 bootstrap realizations and report the 2.5th and 97.5th percentiles of the resulting distributions as descriptive uncertainty intervals. Because only six or seven solar cycles contribute to the respective analyses, these intervals are interpreted as measures of sensitivity to cycle composition rather than as precise population-level confidence limits.

2.7. Sensitivity to Solar Cycle 19 and the year 1961

Solar Cycle 19 was exceptionally strong and may exert substantial influence on relationships derived from historical solar-activity records. We therefore repeat the analysis after excluding Solar Cycle 19. This test evaluates whether the differences between facular and plage scaling depend predominantly on the most active cycle in the investigated period.

A separate sensitivity test excludes observations from the calendar year 1961. This exclusion is motivated by documented residual artifacts in the KoSO Ca II K photographic record around that year (Jha et al. 2024).

We also consider the combined exclusion of Solar Cycle 19 and the year 1961 when evaluating the robustness of the inferred scaling-exponent differences. The primary conclusions are based on comparisons across the full dataset and these restricted subsets, rather than on any single solar cycle or observational year.

3. Results

3.1. Observed area-scaling relationships

The analysis comprises 847 monthly records from Solar Cycles 14–20 for which all three area series satisfy the selection criteria described in Section 2. The empirical relationships between corrected sunspot area S and white-light facular area F, and between S and Ca II K plage area P, are shown in Fig. 1. The three fitted relationships are linear, saturating, and power-law functions. The left-hand panels use all seven cycles, while the right-hand panels exclude Cycle 19.

For faculae, the fitted saturating and power-law curves rise less steeply than the linear relation at large S. The difference is especially apparent in the full-cycle fit, where the linear model continues to increase while the saturating model progressively flattens. The plage curves also exhibit sublinear behaviour, but their separation is less pronounced over much of the observed range. These curves describe empirical associations; the unconstrained fitted intercepts should not be interpreted as physically meaningful predictions at zero sunspot area.

For the full sample, the fitted power-law exponents are $\alpha_F = 0.382$ and $\alpha_P = 0.710$, giving $\Delta\alpha \equiv \alpha_P - \alpha_F = 0.327$. Thus, the facular-area relationship is more strongly sublinear than the plage-area relationship within the fitted model family.

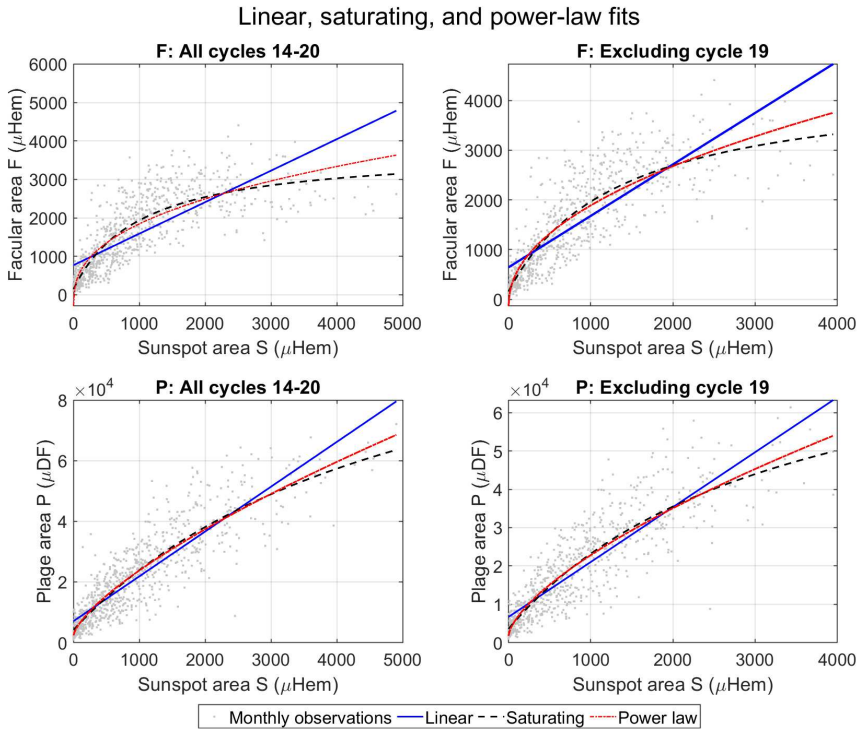


Figure 1. Monthly area-scaling relationships for white-light faculae (top) and Ca II K plage (bottom) as functions of corrected sunspot area. Left: all Solar Cycles 14–20. Right: the sample excluding Cycle 19. Grey points denote monthly observations; blue solid, black dashed, and red dash-dotted curves represent the linear, saturating, and power-law fits, respectively. Sunspot and facular areas are expressed in μHem, whereas plage area is expressed in μDF.

3.2. Predictive performance under leave-one-cycle-out validation

The leave-one-solar-cycle-out (LOCO) comparison provides a more stringent assessment of predictive performance than in-sample fit quality (Fig. 2). With all seven cycles included, the pooled facular LOCO root-mean-square error (RMSE) is 687.9 μHem for the linear model, 520.4 μHem for the saturating model, and 556.8 μHem for the power law. Relative to the linear baseline, these correspond to RMSE reductions of 24.4% and 19.1%, respectively, as quantified by the relative improvement defined in Equation 8. The saturating model therefore gives the lowest facular prediction error among the three tested forms.

For plage, the corresponding pooled LOCO-RMSE values are 7278.0, 7267.0, and 7170.8 μDF. The saturating model improves on the linear baseline by only 0.15%, while the power law improves it by 1.47%. The much smaller changes indicate that the predictive advantage of a nonlinear model is substantially weaker for plage than for white-light faculae. Absolute RMSE values are compared only within each response variable because F and P have different units.

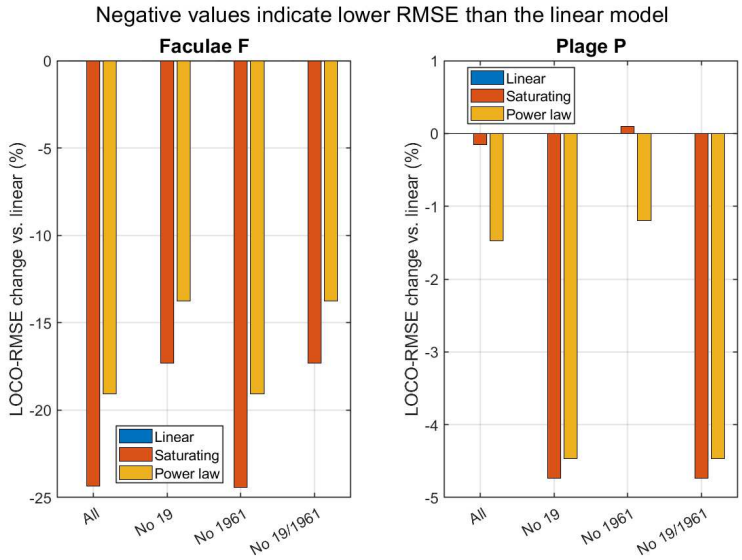


Figure 2. Percentage change in pooled LOCO-RMSE relative to the linear model for facular area (left) and plage area (right). The four samples comprise all cycles, exclusion of Cycle 19, exclusion of 1961, and exclusion of both. Negative values indicate lower RMSE than the linear baseline; the linear model itself has zero change by definition. The different vertical scales emphasize that nonlinear models yield much larger predictive gains for faculae than for plage.

The percentage changes shown in Figure 2 use the opposite sign convention to the improvement measure defined in Equation 8; negative values in the figure therefore indicate improved predictive performance.

3.3. Sensitivity to Cycle 19 and the year 1961

The difference in power-law exponents persists under all examined data exclusions (Fig. 3). Excluding Cycle 19 increases the facular exponent from 0.382 to 0.476 and decreases the plage exponent from 0.710 to 0.661. The resulting exponent difference remains positive, $\Delta\alpha = 0.185$. Excluding 1961 alone produces $\alpha_F = 0.385$ and $\alpha_P = 0.718$, or $\Delta\alpha = 0.333$. Excluding both Cycle 19 and 1961 gives the same point estimates as excluding Cycle 19 alone, because 1961 falls within that cycle.

The LOCO results show a similar contrast in robustness. Without Cycle 19, the saturating model reduces facular RMSE from 630.9 to 521.8 μHem, an improvement of 17.3%. For plage, the corresponding reduction is from 6569.3 to 6258.3 μDF, or 4.7%. Excluding 1961 alone leaves the facular improvement essentially unchanged at 24.4%, while the plage saturating model performs slightly worse than the linear baseline (-0.10% improvement).

The right-hand panel of Fig. 3 shows the facular LOCO-RMSE separately for each held-out cycle. Cycle 19 has the largest error for the linear model, approximately 980 μHem, whereas the saturating and power-law models have substantially lower errors for that cycle. These are out-of-cycle prediction errors,

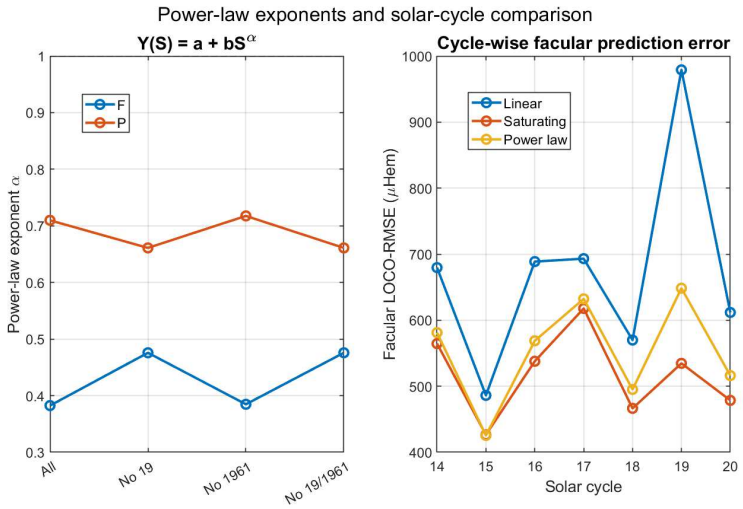


Figure 3. Sensitivity of the fitted power-law exponents and cycle-specific facular prediction errors. Left: fitted power-law exponents for faculae (F) and plage (P) under four data selections. Right: facular LOCO-RMSE for each held-out Solar Cycle 14–20, with each model trained on the remaining cycles. The exponents are fitted on the indicated subsets, whereas the cycle-wise errors are out-of-sample validation results.

not fits trained on the displayed test cycle. The prominence of Cycle 19 helps explain why excluding it reduces the overall advantage of the nonlinear facular models, although the advantage does not disappear.

3.4. Solar-cycle block-bootstrap uncertainty

To assess sensitivity to the composition of the observed cycles, we resampled complete solar-cycle blocks with replacement, using 300 bootstrap realizations (Fig. 4). For the full seven-cycle sample, the observed exponent difference is $\Delta\alpha = 0.327$, with a 95% bootstrap percentile interval of [0.099, 0.472]. The interval remains above zero, consistent with a larger power-law exponent for plage than for faculae across the resampled cycle compositions.

The observed LOCO-RMSE improvement of the saturating facular model is 24.36%, with a 95% percentile interval of [8.05, 41.25]%. For plage, the corresponding improvement is 0.15%, with an interval of [−17.82, 10.78]%. Thus, the bootstrap results do not establish a consistent predictive benefit from saturation for plage. The difference between the facular and plage saturation-model improvements is 24.21 percentage points, with a percentile interval of [4.63, 58.61] percentage points.

The positive exponent difference and the greater facular benefit from the saturating model are also retained when Cycle 19 is excluded: $\Delta\alpha = 0.185$ with percentile interval [0.051, 0.292], and a facula-minus-plage improvement difference of 12.57 percentage points with interval [1.90, 33.36]. Excluding 1961 alone likewise leaves both differences positive. These intervals are descriptive sensitivity summaries rather than precise confidence limits: only seven independent cycle blocks are available in the full sample, and six when Cycle 19 is omitted.

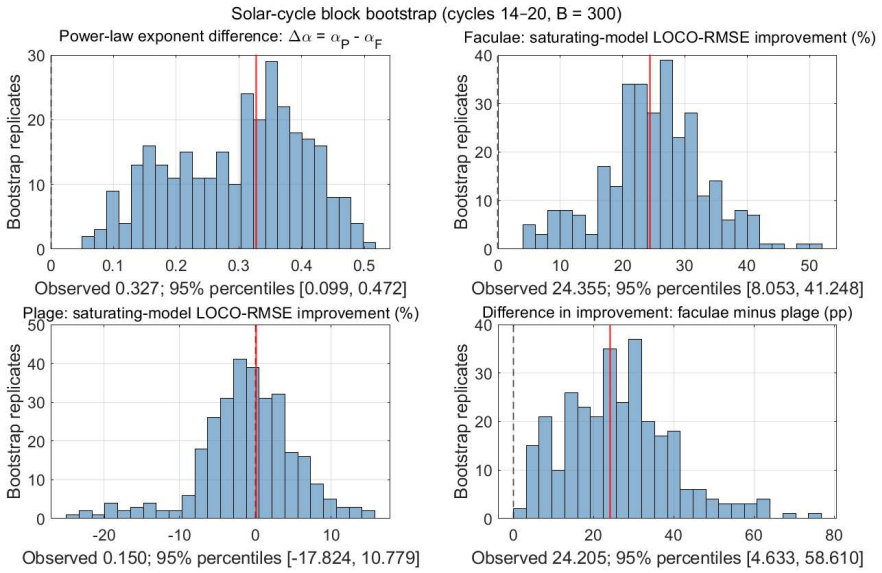


Figure 4. Solar-cycle block-bootstrap distributions for the full sample (Solar Cycles 14–20; 300 resamples). Top left: difference between plage and facular power-law exponents, $\Delta\alpha = \alpha_P - \alpha_F$. Top right and bottom left: percentage improvements in pooled LOCO-RMSE of the saturating model relative to the linear baseline for faculae and plage, respectively. Bottom right: facular minus plage improvement, in percentage points. Red vertical lines indicate observed statistics; black dashed lines indicate zero. The annotations report observed values and 95% bootstrap percentile intervals. Given the small number of independent solar-cycle blocks, these intervals are interpreted descriptively.

4. Discussion

4.1. Different scaling behaviour of faculae and plages

The present analysis reveals a systematic difference between the empirical relationships of white-light facular and Ca II K plage areas with sunspot area. Although both quantities increase with sunspot activity, the facular relationship exhibits stronger sublinear behaviour than the plage relationship. For Solar Cycles 14–20, the fitted power-law exponents are $\alpha_F = 0.382$ and $\alpha_P = 0.710$, respectively.

This difference is also reflected in the predictive performance of the empirical models. Under leave-one-solar-cycle-out validation, the saturating model reduces the facular RMSE by approximately 24% relative to the linear model. For plage area, the corresponding improvement is only 0.15%, while the power-law model provides a modest improvement of approximately 1.5%.

These findings suggest that the relationship between white-light facular area and sunspot area becomes progressively less steep at higher activity levels. In contrast, the plage-area relationship remains closer to linear over the observed range, although its fitted power-law exponent is also below unity. Thus, both relationships may exhibit nonlinearity, but the predictive advantage of nonlinear models is substantially greater for white-light faculae than for Ca II K plages.

The results should not be interpreted as evidence that plage areas follow an exactly linear physical law. Instead, they indicate that the nonlinear models considered here offer relatively little additional out-of-cycle predictive accuracy for plage area compared with their substantial advantage for white-light facular area.

The fitted plage exponent should not be interpreted as a universal scaling index, since previous work has demonstrated that the inferred relationship depends on the observational dataset and temporal aggregation (Chatzistergos et al. 2022a).

4.2. Possible physical and observational origins

The different scaling relationships may reflect, at least in part, the distinct observational properties of photospheric white-light faculae and chromospheric Ca II K plages.

The visibility and intensity contrast of photospheric faculae depend on observing geometry and magnetic flux density (Yeo et al. 2013; Albert et al. 2023). Ca II K plages, by contrast, are identified through chromospheric brightness enhancements, and their measured areas depend on the spectral and photometric characteristics of the observations, as well as on the adopted image-processing and segmentation procedures (Chatzistergos et al. 2022b). Consequently, the areas identified in these two diagnostics need not respond identically to changes in solar magnetic activity.

A progressively weaker increase in the measured white-light facular area at high sunspot activity could arise from changes in the relative abundance, spatial distribution, or visibility of bright magnetic structures. Differences in contrast thresholds and historical observing procedures could also contribute to the observed curvature. The present analysis cannot distinguish these possibilities quantitatively. In particular, the empirical saturating model should not be interpreted as direct evidence for a specific physical saturation mechanism. Establishing such a mechanism would require additional information about magnetic flux, feature contrast, and observing geometry.

The distinction between facular and plage scaling is nevertheless relevant to studies of solar brightness variability. Photospheric and chromospheric area indices are often used as complementary indicators of magnetic activity, but their relationships with sunspot area should not be assumed to have identical functional forms.

4.3. Influence of Solar Cycle 19

Solar Cycle 19 provides an important test of the stability of the inferred relationships. Its exceptionally high activity extends the observed sunspot-area range and therefore has substantial leverage on the fitted nonlinear models.

When Cycle 19 is excluded, the facular power-law exponent increases from 0.382 to 0.476, while the plage exponent decreases from 0.710 to 0.661. The exponent difference remains positive, however, with $\Delta\alpha = 0.185$.

The predictive advantage of the saturating facular model also persists after excluding Cycle 19, although its LOCO-RMSE improvement decreases from

approximately 24% to 17%. For plage, the corresponding improvement increases from 0.15% to approximately 4.7%.

The cycle-specific validation results show that Cycle 19 is particularly difficult to predict using the linear facular model. This contributes to the strong overall advantage of the nonlinear facular models in the full sample.

Nevertheless, the persistence of the exponent difference and the facular predictive improvement after removing Cycle 19 indicates that the principal contrast between the two diagnostics is not solely a consequence of this exceptionally active cycle.

4.4. Historical data limitations and uncertainty

Several limitations should be considered when interpreting these results. First, the Greenwich white-light facular record is a historical observational series with known concerns regarding consistency and interpretation (Foukal 1993). Its measured areas may be affected by observing conditions, feature visibility, and changes in measurement procedures. Such effects could influence the apparent nonlinearity of the facular relationship.

Second, the KoSO Ca II K plage series depends on the processing and calibration of historical photographic observations. Residual image artifacts and temporal inhomogeneities remain possible despite the corrections applied to the archive (Jha et al. 2024). Excluding the year 1961, which has been identified as a potentially problematic period, does not materially change the main conclusions.

Third, the monthly values of the three quantities do not necessarily represent observations obtained on identical days. The sunspot and white-light facular series were matched at the daily level before monthly averaging, whereas the KoSO plage series was joined by calendar month. This construction supports comparisons of monthly activity but may introduce additional scatter into the area–area relationships.

The original area units were retained: μHem for sunspot and facular areas and μDF for plage areas. Accordingly, the comparison focuses on scaling exponents and relative predictive improvements rather than absolute area values or RMSE magnitudes across the two response variables.

Finally, the analysis contains only seven solar cycles. Although the dataset comprises 847 monthly observations, these months are not independent realizations of long-term solar-cycle behaviour. The solar-cycle block bootstrap addresses this limitation by resampling complete cycles rather than individual months. For the full sample, the 95% percentile interval for the exponent difference is [0.099, 0.472], while the interval for the difference between facular and plage saturation-model improvements is [4.63, 58.61] percentage points. Both intervals are positive, supporting the observed contrast across the resampled cycle compositions. However, because only seven independent cycle blocks are available, these intervals should be regarded as descriptive sensitivity measures rather than precise population-level confidence limits.

The original Greenwich Photo-Heliographic Results show that the observational network and measurement procedures evolved over the history of the series. For example, the 1940 volume reports that most photographs were measured

once, whereas the 1955 volume states that all photographs were measured independently by two observers (Royal Observatory, Greenwich 1952; Royal Greenwich Observatory 1958). Such differences underline the need for caution when interpreting long-term changes in measured facular areas.

4.5. Implications and further work

The results demonstrate the importance of evaluating photospheric and chromospheric area indices separately when constructing empirical relationships with sunspot activity.

For the historical data examined here, a saturating relationship provides a substantial improvement in predicting white-light facular area across solar cycles. The corresponding improvement for Ca II K plage area is much smaller, and the preferred nonlinear form is less clearly distinguished from a linear baseline.

Further investigation using independent facular and plage archives would help establish whether this contrast is specific to the historical records considered here or represents a more general property of solar magnetic activity diagnostics. Comparisons with modern observations that include simultaneous magnetic-field measurements could also help separate physical changes in magnetic structures from diagnostic-dependent visibility and measurement effects.

5. Conclusions

We compared the scaling relationships of historical white-light facular and Ca II K plage areas with corrected sunspot area over Solar Cycles 14–20, using 847 monthly observations.

Three empirical models were examined: linear, saturating, and power-law relationships. Their predictive performance was evaluated using leave-one-solar-cycle-out validation, with additional sensitivity tests and solar-cycle block bootstrap resampling.

The main findings are as follows.

i) The facular-area relationship is more strongly sublinear than the plage-area relationship. The fitted power-law exponents are $\alpha_F = 0.382$ and $\alpha_P = 0.710$, giving $\Delta\alpha = 0.327$.
ii) The saturating model provides the lowest facular LOCO-RMSE, reducing the prediction error by approximately 24% relative to the linear model. For plage area, the corresponding improvement is only 0.15%, while the power-law model improves the RMSE by approximately 1.5%.
iii) The principal differences persist after excluding Solar Cycle 19 and after excluding the year 1961. Cycle 19 nevertheless contributes substantially to the predictive advantage of nonlinear facular models.
iv) Solar-cycle block bootstrap resampling yields positive percentile intervals for both the difference in power-law exponents and the difference in saturation-model predictive improvements. These intervals are interpreted descriptively because the analysis contains only seven solar cycles.

Overall, the results indicate that white-light facular and Ca II K plage areas exhibit distinct empirical scaling relationships with sunspot area. In particular, nonlinear saturation provides a substantially greater predictive benefit for historical white-light facular areas than for Ca II K plage areas. These differences should be taken into account when using historical area indices to characterize solar magnetic activity and its variability.

Acknowledgements

The author acknowledges the Royal Greenwich Observatory and the contributing observatories for the historical sunspot and white-light facular observations. The author also acknowledges the Kodaikanal Solar Observatory and the researchers involved in digitizing, calibrating, and maintaining the historical Ca II K observations. The authors of the cross-calibrated sunspot-area catalogue and the processed Kodaikanal plage-area series are gratefully acknowledged for making these historical solar-activity records available to the research community.

Data Availability

The sunspot-area data used in this study are based on the cross-calibrated catalogue of Mandal et al. (2020). The white-light facular areas were obtained from the historical Greenwich Photo-Heliographic Results, and the Ca II K plage areas from the processed Kodaikanal Solar Observatory series described by Jha et al. (2024). The monthly dataset assembled for this study and the analysis code are available from the author upon reasonable request.

Funding

The author received no specific funding for this work.

Competing Interests

The author declares no competing interests.

References

K. Albert, N. A. Krivova, J. Hirzberger, S. K. Solanki, A. Moreno Vacas, D. Orozco Suárez, et al. Intensity contrast of solar network and faculae close to the solar limb, observed from two vantage points. *Astronomy & Astrophysics*, 678:A163, 2023. doi: 10.1051/0004-6361/202346037.

T. Chatzistergos, I. Ermolli, N. A. Krivova, S. K. Solanki, D. Banerjee, et al. Analysis of full-disc Ca II K spectroheliograms. III. plage area composite series covering 1892–2019. *Astronomy & Astrophysics*, 639:A88, 2020. doi: 10.1051/0004-6361/202037746.

T. Chatzistergos, I. Ermolli, N. A. Krivova, T. Barata, S. Carvalho, and J.-M. Malherbe. Scrutinising the relationship between plage areas and sunspot areas and numbers. *Astronomy & Astrophysics*, 667:A167, 2022a. doi: 10.1051/0004-6361/202244913.

T. Chatzistergos, N. A. Krivova, and I. Ermolli. Full-disc Ca II K observations: A window to past solar magnetism. *Frontiers in Astronomy and Space Sciences*, 9:1038949, 2022b. doi: 10.3389/fspas.2022.1038949.

T. Chatzistergos, N. A. Krivova, and K. L. Yeo. Long-term changes in solar activity and irradiance. *Journal of Atmospheric and Solar-Terrestrial Physics*, 252:106150, 2023. doi: 10.1016/j.jastp.2023.106150.

P. Foukal. The curious case of the greenwich faculae. *Solar Physics*, 148(2):219–232, 1993. doi: 10.1007/BF00645087.

P. Foukal. The behavior of solar magnetic plages measured from Mt. Wilson observations between 1915–1984. *Geophysical Research Letters*, 23(16):2169–2172, 1996. doi: 10.1029/96GL01356.

P. Foukal and J. Lean. An empirical model of total solar irradiance variation between 1874 and 1988. *Science*, 247(4942):556–558, 1990. doi: 10.1126/science.247.4942.556.

B. K. Jha, T. Chatzistergos, D. Banerjee, I. Ermolli, N. A. Krivova, S. K. Solanki, and A. Priyadarshi. Butterfly diagram and other properties of plage areas from kodaikanal Ca II K photographs covering 1904–2007. *Solar Physics*, 299(12):166, 2024. doi: 10.1007/s11207-024-02408-6.

S. Mandal, S. Chatterjee, and D. Banerjee. Association of plages with sunspots: A multi-wavelength study using kodaikanal Ca II K and greenwich sunspot area data. *The Astrophysical Journal*, 835(2):158, 2017. doi: 10.3847/1538-4357/835/2/158.

S. Mandal, N. A. Krivova, S. K. Solanki, N. Sinha, and D. Banerjee. Sunspot area catalogue revisited: Daily cross-calibrated areas since 1874. *Astronomy and Astrophysics*, 2020. doi: 10.1051/0004-6361/202037547.

M. Priyal, J. Singh, B. Ravindra, T. G. Priya, and K. Amareswari. Long term variations in chromospheric features from Ca-K images at kodaikanal. *Solar Physics*, 289(1):137–152, 2014. doi: 10.1007/s11207-013-0315-7.

Royal Greenwich Observatory. *Greenwich Photo-heliographic Results, 1955*. Her Majesty's Stationery Office, London, 1958. Results of measures of photographs of the Sun taken at Herstmonceux, the Cape, and Kodaikanal in the year 1955.

Royal Observatory, Greenwich. *Photo-heliographic Results, 1874 to 1885: Supplementary Results from Photographs of the Sun*. His Majesty's Stationery Office, Edinburgh, 1907. Appendix to the Greenwich Observations, 1905.

Royal Observatory, Greenwich. *Greenwich Photo-heliographic Results, 1940*. Her Majesty's Stationery Office, London, 1952. Results of measures of photographs of the Sun taken at Greenwich, the Cape, and Kodaikanal in the year 1940.

S. K. Solanki, B. Inhester, and M. Schüssler. The solar magnetic field. *Reports on Progress in Physics*, 69(3):563–668, 2006. doi: 10.1088/0034-4885/69/3/R02.

K. L. Yeo, S. K. Solanki, and N. A. Krivova. Intensity contrast of solar network and faculae. *Astronomy & Astrophysics*, 550:A95, 2013. doi: 10.1051/0004-6361/201220682.

K. L. Yeo, S. K. Solanki, and N. A. Krivova. How faculae and network relate to sunspots, and the implications for solar and stellar brightness variations. *Astronomy & Astrophysics*, 639: A139, 2020. doi: 10.1051/0004-6361/202037739.